Biomed Microdevices (2008) 10:839–849
DOI 10.1007/s10544-008-9198-z

Micro-well texture printed into PEG hydrogels using the FILM nanomanufacturing process affects the behavior of preadipocytes

David Y. Fozdar · Xuemei Wu · Charles W. Patrick Jr. · Shaochen Chen

Published online: 17 June 2008

Abstract To date, biomaterial scaffolds for adipose tissue engineering have focused on macro- and upper micro-scale fabrication, biocompatibility, and biodegradation, but have failed to recapitulate the sub-micron dimensions of native extracellular matrix (ECM) and, therefore, have not optimized material–cell interactions. Here, we report the findings from a study investigating the effects of a quasi-mimetic sub-micron (<1 μm) surface texture on the qualitative behavior of preadipocytes (PAs). We found that PAs in contact with tread-like micro-well structures exhibit a different morphology relative to PAs seeded onto control smooth glass surfaces. Additionally, the micro-well topography induced isolated PAs to undergo adipogenesis, which usually occurs in the presence of aggregates of contact-inhibited PAs. The micro-well structures were printed into polyethylene glycol dimethacrylate (PEGDMA) using the recently reported nanomanufacturing process called *F*lash *I*mprint *L*ithography Using a *M*ask Aligner (FILM). FILM is a simple process that can be utilized to fabricate micro- and nanostructures in UV-curable materials (D.Y. Fozdar, W. Zhang, M. Palard, C.W. Patrick Jr., S.C. Chen, Flash Imprint Lithography Using A Mask Aligner (FILM): A Method for Printing Nanostructures in Photosensitive Hydrogels for Tissue Engineering. Nanotechnology **19**, 2008). We demonstrate the utilization of the FILM process for a tissue engineering application for the first time. The micro-well topographical theme is characterized by contact angle and surface energy analysis and the results were compared with those for smooth glass and unpatterned PEGDMA surfaces. Based on our observations, we believe that the micro-well texture may ultimately be beneficial on implantable tissue scaffolds.

Keywords Adipose tissue engineering · Nanomanufacturing · Polyethylene glycol · Preadipocyte · Tissue scaffold

D. Y. Fozdar · S. Chen (✉)
Department of Mechanical Engineering,
Center for Nano Molecular Science and Technology,
Microelectronics Research Center,
The University of Texas at Austin,
1 University Station, C2200,
Austin, TX 78712, USA
e-mail: scchen@mail.utexas.edu

D. Y. Fozdar
e-mail: davidfozdar@mail.utexas.edu

X. Wu · C. W. Patrick Jr.
Department of Biomedical Engineering,
The University of Texas M.D. Anderson Cancer Center,
1515 Holcombe Blvd., Unit 193,
Houston, TX 77030, USA

1 Introduction

Adipose tissue engineering, the field of growing new vascularized adipose tissue, has great potential in repairing soft tissue deficits resulting from congenital abnormalities (e.g., hemifacial microsomia, Parry Romberg's syndrome, and Poland's syndrome), trauma, and tumor resection (Wang et al. 2005). These contour defects can be psychologically devastating to patients and, in many cases, physical impairments also result (e.g., loss of range of motion). Current reconstructive treatments consist of implanting or injecting synthetic materials or injecting autologous fat tissue (fat tissue removed from other parts of the patient's own body; Wang et al. 2005; Hunt and Hobar 2003; Vaienti et al. 2005; Asai et al. 2006). These treatments are far from ideal. Implanted or injected synthetic materials often induce immune responses dire to

the patient, while injected autologous fat tissue is resorbed by the body causing a 40–60% reduction in graft volume (Billings and May 1989; Ersek 1991). All conventional treatments only correct volume deficits of defects and do not correct for concomitant losses in function (e.g., loss of range of motion). A new promising strategy for treating soft-tissue defects is to fundamentally grow new fully-functioning vascularized adipose (fat) tissue on biomaterial scaffolds. This particular area of research, focused at growing new adipose tissue, is called adipose tissue engineering.

Adipose tissue engineering involves a minimum of three components, a tissue scaffold providing the necessary boundary conditions for tissue formation, pertinent cell types that can be cultured to form new adipose tissue, and a permissive microenvironment (Patrick 2000, 2001). The microenvironment consists of physical and chemical cues that influence the behavior and proliferation of the pertinent cells. To grow new adipose tissue, the appropriate cells are seeded onto a tissue scaffold, which ultimately controls 3D tissue morphology, and the cells proliferate and differentiate into fully-functioning vascularized adipose tissue. To date, biomaterial scaffolds for adipose tissue have focused on macro- and upper micro-scale fabrication, biocompatibility, and biodegradation. They have failed to recapitulate the microscale dimension of native extracellular matrix (ECM) and, therefore, have not optimized material–cell interactions. Significant progress has been made in using preadipocytes (PAs), precursor adipose cells that differentiate into mature fully-differentiated adipose cells, to form new adipose tissue. PAs can readily be expanded *ex vivo*, unlike fully-differentiated adipose cells, and the process by which they differentiate into mature adipose cells, called adipogenesis, is largely understood.

Although the process of adipogenesis is well-understood, physical stimuli causing the onset of adipogenesis and other behavior of preadipocytes, remains largely unknown. In vivo, preadipocytes are surrounded by an ECM that is patterned down to sub-micron scales (<1 μm; Sniadecki et al. 2006; Abrams et al. 2000; Yim et al. 2005). Accordingly, mimicking the ECM in implantable biomaterial scaffolds may be very important in elucidating certain responses of PAs that are important in the development of healthy new adipose tissue. In order to truly harness PA-response, specific topographical schemes have to be strategically designed and manufactured, physically characterized (e.g. contact angle and surface energy analysis), and interactions between the texture and PAs have to be monitored in culture.

Just like tires have tread to help a car gain traction to the road and a bathtub has rubber grips to prevent slipping, we show that periodic tread-like micro-well structures patterned into polyethylene glycol (PEG) hydrogels mediate interactions that affect the morphology of PA's. We chose the micro-well topographical theme based on the idea that the texture would enhance contact with PAs in culture and induce an atypical cell-response. We fabricate the micro-well texture in PEG-dimethacrylate (PEGDMA) by a nanomanufacturing process recently developed by our group called *F*lash *I*mprint *L*ithography using a *M*ask Aligner (FILM) (Fozdar et al. 2008). PEGDMA is a biocompatible liquid polymer that can be made to solidify upon exposure to ultraviolet light (365 nm *i*-line UV). PEGDMA has optimal material and chemical properties that make it ideal for use in actual three-dimensional implantable adipose tissue scaffolds.

The FILM process is an alternative to Step-and-Flash Imprint Lithography (S-FIL) and other variations of UV-Nanoimprint Lithography (UV-NIL). S-FIL is a very promising technology that is currently being adapted to semiconductor electronics fabrication; however, it requires the use of unconventional dedicated nanoimprinting tools (Colburn et al. 1999). Such dedicated imprinting tools are typically unavailable in most clean rooms and require extremely costly quartz imprinting templates and ad hoc drop dispensers to support different photosensitive materials. The FILM process requires the use of a common mask aligner normally used for photolithography, cheap silicon imprinting molds, and can be used with any low-viscosity UV-curable biomaterial. FILM was developed as a more suitable alternative for fabricating structures in UV-curable materials with nanoscale resolution (<100 nm) than photolithography, S-FIL, and general UV-nanoimprint lithography (UV-NIL). Here, we demonstrate the use of the FILM process for a tissue engineering application for the first time.

The interactions observed between PAs and the micro-well topography exemplify the need for incorporating sub-micron strategically designed (<1 μm) surface textures in implantable biomaterial adipose tissue scaffolds. Furthermore, we believe that the micro-well topography studied in our investigations may be beneficial on implantable adipose tissue scaffolds.

2 Materials and methods

2.1 Synthesis of PEGDMA biomaterial

PEGDMA prepolymer of MW=1,000 (Polysciences Inc., Warrington, PA, USA, No. 25852-47-5) was dissolved in HPLC-grade demineralized water (Fisher Chemical, Fairlawn, NJ, USA, No. 7732-18-5) to a concentration of 100% (*w*/*v*). Irgacure 2959 photoiniator (Ciba Specialty Chemicals, Tarrytown, NY, USA) was added to the PEGDMA/water mixture to a concentration of 0.1% (*w*/*v*) relative to the volume of water used (e.g., 0.001 g of Irgacure pure 1 mL of

water). The PEGDMA was centrifuged for 30 min and refrigerated overnight to allow the mixture to stabilize.

2.2 Fabrication of silicon molds

Silicon wafers (NOVA Electronic Materials, Richardson, TX, USA) were diced into 20 mm×20 mm pieces. The silicon pieces were ashed in an O_2-plasma asher (March CS-1701, March Plasma Systems, Concord, CA, USA) to burn off organic contaminants, cleaned in a mixture of 30% H_2O_2 (*v*/*v*) in H_2SO_4 (piranha solution; Hydrogen Peroxide 30%—No. 2190, Sulfuric Acid 96%—No. 9684, J.T. Baker, Phillipsburg, NJ, USA) for 8 min, and washed thoroughly in DI water. The wafer pieces were dried thoroughly with N_2 and then dehydration-baked at 200°C for 5 min on a hot plate to remove all residual moisture. A 20-nm silicon dioxide layer was deposited on the clean silicon using plasma-enhanced chemical vapor deposition (PECVD; Plasma-Therm 790, Plasma-Therm, Inc., St. Petersburg, FL, USA). ZEP-520A (Zeon Chemicals, Louisville, KY, USA) positive electronic resist was thinned in Anisole to a 1:3 ratio (*v*/*v*), respectively; ZEP-520A resist was chosen due to its high resolution and dry-etch resistance. The resist was deposited on the molds by spin-coating at 4,000 rpm for 60 s to a thickness of approximately 100 nm and then soft-baked at 180°C for 90 sec. The resist was patterned using electron beam lithography (EBL; JEOL 6000 FSE, JEOL Ltd., Tokyo, Japan; Raith 50, Raith GmbH, Dortmund, Germany) and developed in ZED-N50 solution (Zeon Chemicals, Louisville, KY, USA). The patterned samples were descummed in an O_2-plasma to remove residual resist in the developed regions of the resist. Exposed silicon dioxide was etched through by RIE (Plasma-Therm 790, Plasma-Therm, Inc., St. Petersburg, FL, USA) using the resist as a mask. The resist was subsequently stripped in 30% H_2O_2 (*v*/*v*) in H_2SO_4. The exposed underlying silicon was etched with RIE using the patterned silicon dioxide layer as a mask. The silicon dioxide layer was then removed in buffered oxide etchant (BOE) leaving the patterned silicon.

2.3 Chemical pretreatment of silicon molds

Silicon molds were chemically treated with Tridecafluoro-1,1,2,2-Tetrahydrooctyl-1 Trichlorosilane (United Chemical Technologies, Inc., Bristol, PA, USA, No. T2492). The silicon molds were ashed in an O_2-plasma asher to burn of organic contaminants and then immersed in a mixture of 30% H_2O_2 (*v*/*v*) in H_2SO_4 for 10 min, washed thoroughly in DI water, dried thoroughly with N_2, and dehydration-baked at 200°C for 5 min on a hot plate. The clean silicon molds were then placed in a small container in juxtapose to a small vial containing a few drops of the fluorinated-silane. The container was then covered and stored in a dehumidified nitrogen environment to prevent any reactions between the fluorinated-silane and ambient moisture. After 4 h, the silicon molds were removed and washed with a mixture of 25% carbon tetrachloride (*v*/*v*) in heptane and sequentially sonicated in acetone, methanol, and isopropyl alcohol (IPA; Acetone Certified ACS, methanol Certified ACS, 2-Propanol Certified ACS, Fisher Chemical, Fairlawn, NJ, USA) for 5 min each. In between imprints using the mask aligner, residual photopolymerized PEGDMA was removed from the silicon molds by sequential immersion in acetone, methanol, and IPA for 1 min each. After being chemically treated with the fluorinated-silane, the silicon molds were dried after each rinse with N_2 but never baked in an effort to preserve the silane layer.

2.4 Chemical pretreatment of glass microscope slides

Glass microscope slides were immersed in a mixture of 30% H_2O_2 (*v*/*v*) in H_2SO_4 for 10 minutes, washed thoroughly in DI water, dried thoroughly with N_2, and immersed in a 1 mM solution of 3-trichlorosilyl propyl methacrylate (TPM) in a mixture of 25% carbon tetrachloride (*v*/*v*) in heptane for 5 min. The piranha solution is a strong oxidizer that cleaned and hydroxylated the microscope slides; the silane attached to the hydroxyl groups (–OH) on the surface of the glass. Since TPM is highly reactive towards water, the microscope slides were meticulously dried before immersion in the silane solution. Because it was extremely difficult to remove all the residual moisture on the microscope slides using N_2 alone, the microscope slides typically formed a powdery-like surface when in contact with the silane solution. The powdery residue formed when the silane reacted with the residual moisture on the microscope slides that was not removed by the N_2. Moreover, unless the silane solution was kept in a dehumidified environment, moisture from the air often caused large particles to form in the silane solution that attached to the microscope slides. To limit the amount of powdery-like residue that formed and attached to the surface of the glass microscope slides, the silane mixture was stirred for the 5-min duration in which the microscope slides were immersed. Upon removing the microscope slides from the silane mixture, the silanized slides were copiously rinsed with a TPM-free mixture of 25% carbon tetrachloride (*v*/*v*) in heptane and then with 1× phosphate buffered saline (PBS). After rinsing, the microscope slides were dried with N_2 and stored in a vacuum dessicator. Carbon tetrachloride served to degrease superfluous silane that did not covalently bond to the silicon surface and remove particulate matter; excess silane was nearly impossible to remove with standard organic solvents like acetone, methanol, and IPA. Pretreated glass slides were dried with N_2 after rinsing but were not dehydration-baked. Baking tended to degrade the tethered

methacrylate groups on the glass slides which reduced PEGDMA adhesion.

2.5 Imprinting of micro-wells in PEGDMA

The micro-well topography was imprinted into PEGDMA using the FILM process, which is illustrated in Fig. 1. First, a silicon mold containing a 1 mm×1 mm area of micro-wells was fabricated using EBL and RIE. The mold was then treated with a fluorinated silane to increase hydrophobicity and a drop of PEGDMA was dispensed on the patterned area. The silicon mold with the PEGDMA droplet was put in a vacuum desiccator at room temperature and a pressure of 0.1 Torr for 10 min to suction the polymer into the features of the mold. The silicon mold was then loaded onto the substrate holder in a mask aligner normally used for photolithography (SUSS MA-6, SUSS Microtech, Munich, Germany) and a 12.7 cm×12.7 cm blank quartz plate was loaded into the mask holder in the aligner (instead of a quartz-chrome photomask). Before loading the dummy plate, a glass microscope slide was treated with a tethered silane and attached to the quartz dummy plate with double-stick tape. After loading the silicon mold and glass substrate, the aligner brought the mold and glass slide together to a prescribed gap-spacing of 5 μm causing the PEGDMA to spread. After letting the PEGDMA spread for about 30 s, the PEGDMA was exposed through the quartz dummy plate for 45 s with 365 nm *i*-line monochromatic UV-light. Finally, the aligner electronically separated the mold from the glass slide leaving the patterned PEGDMA on the glass slide. The FILM process is reported in great detail in reference (Fozdar et al. 2008).

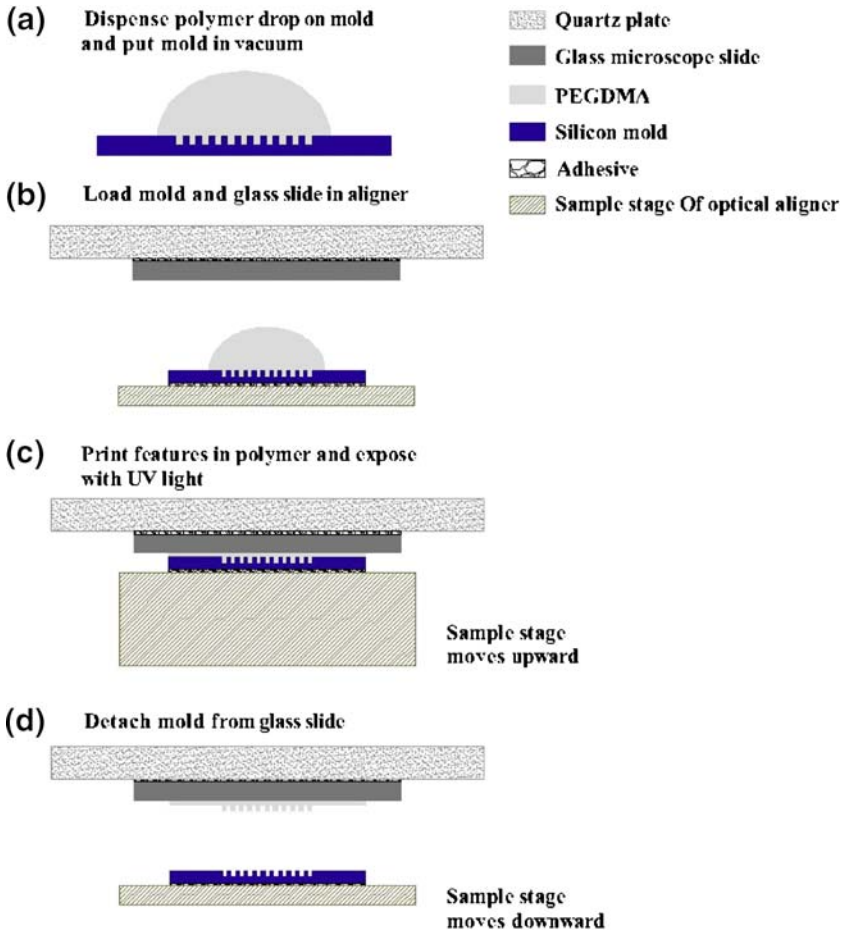

Fig. 1 A schematic diagram of the FILM process. The FILM process utilizes a common mask aligner to print features from cheap silicon molds onto glass microscope slides. (**a**) A drop of UV-curable PEGDMA is dispensed onto a silane-treated silicon mold. The mold is placed into a vacuum desiccator at room temperature and a pressure of 0.1 Torr for 5–10 min. (**b**) The mold is positioned on the motorized sample stage of the aligner using an adhesive (e.g., double-stick tape). Likewise, a silane-treated glass microscope slide is positioned on a quartz plate using an adhesive. The quartz plate adheres to a mask holder (not drawn) by suction and serves as a transparent dummy mask. The mask holder mounts into the aligner. (**c**) The motorized sample stage moves upward until the mold and glass slide come together causing the PEGDMA to spread. The final gap-spacing between the mold and slide can be adjusted depending on the desired gap spacing. Exposure by UV occurs from the top through the quartz plate and glass slide. (**d**) The motorized sample stage detaches the mold from the glass slide leaving the pattern on the slide

2.6 Examination of micro-wells in PEGDMA

Topological features imprinted in PEGDMA were examined using a field-emission scanning-electron microscope (FESEM) (LEO 1530, Carl Zeiss SMT Inc., Peabody, MA, USA) and atomic force microscope (AFM; Dimension 3100 with Microscope IV controller, Digital Instruments & Veeco Metrology Group, Santa Barbara, CA, USA). AFM images were taken using a silicon tip in tapping-mode (Tap300, Budget Sensors, Sophia, Bulgaria).

2.7 Examination of contact angles

Contact angle measurements were taken using a goniometer (FTÅ200, First Ten Angstroms, Inc., Portsmouth, VA, USA). Substrates were placed onto a manually-adjustable sample stage and oriented appropriately; camera lighting, brightness, and contrast were optimized. Small droplets of DI water were electronically dispensed onto the substrates using a syringe pump controlled by computer. Each image was taken a few seconds after a droplet was dispensed. The baseline of the droplets was determined using a reflection image produced when the substrates were slightly tilted. The curvature of the droplets was traced using a non-spherical fit model. Multiple contact angle measurements were taken on each surface to verify accuracy and precision of contact angle data; the number of contact angle measurements (n) taken on each surface is as follows: n=12 for glass; n=8 unpatterned (bare) PEGDMA; n=30 for PEGDMA micro-well surface. Measurements are reported as mean values with a corresponding standard deviation (SD). Information regarding contact angle measurements can be found in the references (Adamson 1982; Andreas et al. 1938; Girifalco and Good 1957; Fowkes and Harkins 1940; Adamson et al. 1970).

2.8 Culture of PAs

Rat PAs were harvested and cultured as previously described (Patel et al. 2005; Patrick et al. 1999, 2002). Control cultures were grown in parallel with all experiments to ensure correct cell phenotype. PAs were not employed greater than passage 2.

2.9 Examination of PAs on micro-well surface

The interactions of PAs on patterned surfaces were examined using a JEM 1010 transmission electron microscope (TEM, JEOL USA, Inc., Peabody, MA) equipped with a digital camera and a JSM 5900 scanning electron microscope (SEM, JEOL USA, Inc., Peabody, MA) equipped with electron backscatter detector and digital camera.

3 Results and discussion

3.1 PEGDMA micro-wells and the FILM process

A schematic of the FILM process used to pattern the micro-well texture in PEGDMA on glass microscope slides is shown in Fig. 1. Figure 2 shows SEM and AFM images of the micro-well texture. The micro-wells consist of an offset array of approximately 500 nm×4 μm wells (the small side is slightly greater than 500 nm). The depth of the micro-wells is approximately 400 nm and the thickness of the residual layer of PEGDMA in Fig. 2(a) is approximately 5 μm so that no portion of the glass microscope slide substrate is exposed in the micro-wells. The depth of the micro-wells can be adjusted based on the depth etched into the silicon molds. Though we utilize a residual layer of 5 μm, the residual layer thickness can be set by controlling the final gap-spacing between the silicon mold and transparent substrate (e.g., glass microscope slides); the aligner has the capability of producing a residual layer of negligible thickness (contact print) to thicknesses upwards of tens of microns. As can be seen in Fig. 2, the FILM process is able to imprint a dense array of high-fidelity microstructures over large areas, which is very important in performing cell studies. The micro-wells have a slightly inward sloping vertical profile, which is a mechanism of the

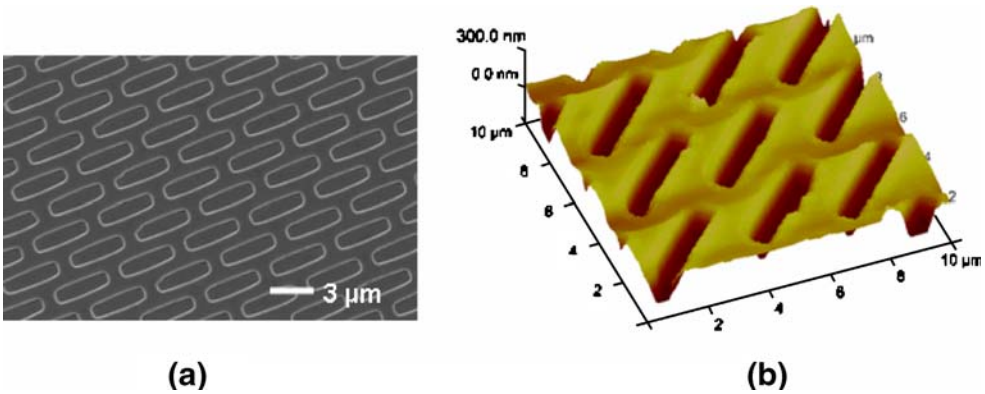

Fig. 2 An (**a**) SEM and (**b**) AFM image of the PEGDMA micro-wells, which consist of an offset array of 500 nm×4 μm wells. The micro-wells were imprinted using the FILM process

sidewall profile of the silicon mold; sidewall profile is controllable during silicon etching in mold fabrication. The slightly inward sloping profile helps facilitate the imprinting process.

One of the most important aspects of FILM is proper substrate chemical-derivatization (Sections 2.3. and 2.4.). Silicon molds were treated with a fluorinated-silane that made the surface rather hydrophobic (contact angle= 104.2°; SD=3.1°) to prevent sticking. Glass microscope slides were treated with a tethered silane (contact angle= 75.0°; SD=6.5°) that attached to the acrylate groups in the PEGDMA upon polymerization by UV. Without proper surface treatment, the PEGDMA almost always delaminated from the glass slides. For some applications, delamination of a patterned sheet of PEGDMA may be desirable, for example, for obtaining implantable two-dimensional adipose tissue scaffolds for replacing thin layers of adipose tissue between skin and muscle.

As ECM *in vivo* comprises topography at sub-micron scales (<1 μm), we hypothesized that PAs would respond to our quasi-mimetic micro-well scheme relative to smooth surfaces. The FILM process was very convenient in performing our study because it allowed us to imprint the micro-wells without using proprietary highly-dedicated imprinting technologies (e.g. IMPRIO 55, 100, and 250 by Molecular Imprints, Austin, TX). While dedicated imprinting technology works well, it is usually inaccessible to most tissue engineers and requires the use of expensive add-ons, molds, and polymer drop dispensers. We also found FILM to be cheaper and easier than photolithography since we didn't require an expensive quartz-chrome photomask; accordingly, issues resulting from the contact between a photomask and PEG (or any UV-curable material) is not an issue in FILM. Even if a quartz-chrome photomask is chemically-treated, contact between the photomask and hydrogel would degrade the chrome features of the mask over time as some sticking occurs between the hydrogel and mask. Because spin-coating low-viscosity hydrogels is extremely difficult, especially on chemically-treated substrates (e.g., a chemically modified glass microscope slide), polymer spreading on a substrate for patterning is usually accomplished naturally as the photolithographic mask aligner brings the substrate and photomask together; thus, contact between the hydrogel and photomask is imminent. Additionally, though our tread-like micro-well structures have a sub-micron width (the small side is slightly greater than 500 nm) that isn't quite nanoscale (<100 nm), FILM has the capability of imprinting nanostructures, which 365 nm *i*-line photolithography cannot produce.

3.2 Contact angle of water on PEGDMA micro-well surface

To characterize changes in hydrophobicity due the presence of the physical microstructures in the PEGDMA, we measured the contact angle of water on the microtextured PEGDMA, unpatterned PEGDMA, and a bare glass microscope slide. Figure 3 illustrates the results of our contact angle measurements. The contact angle of water on

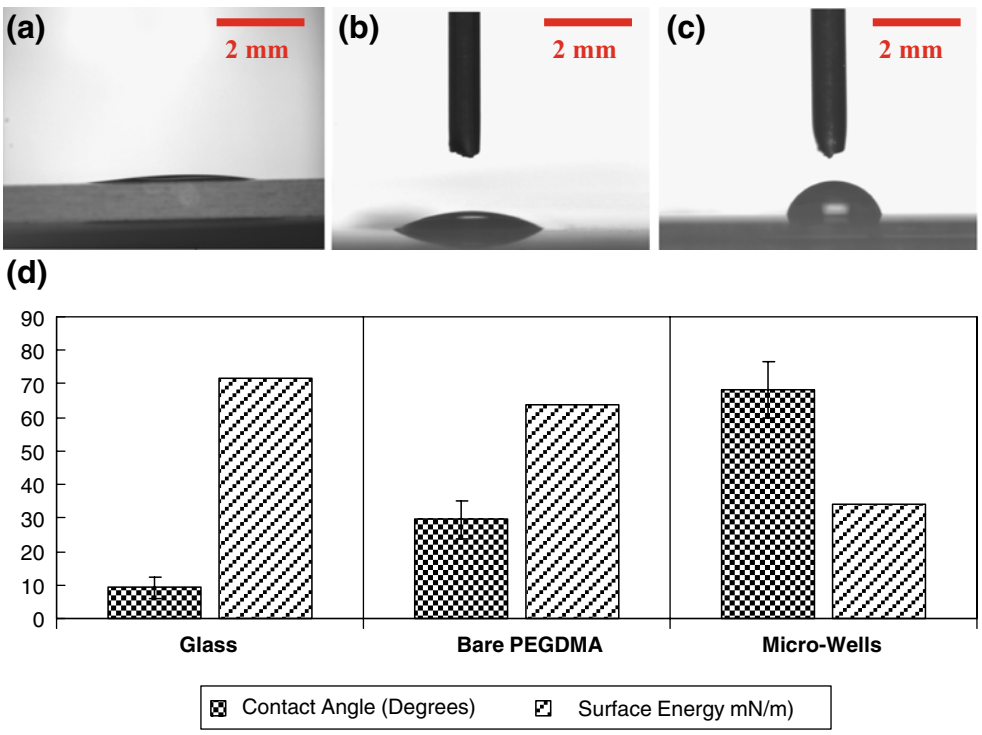

Fig. 3 Contact angle measurements of water on (**a**) glass (9.3°; SD≈3.2°; n=12), (**b**) unpatterned (bare) PEGDMA (29.6°; SD≈5.7°; n=8), and (**c**) PEGDMA patterned with micro-well topography (68.4°; SD≈ 8.4°; n=30). Results for contact angle and associated surface energy calculations are summarized in (**d**); standard deviation for contact angle measurements is illustrated using error bars. The surface energies of glass (γ_{Glass}), bare PEGDMA ($\gamma_{BarePEG}$), and the micro-well surface (γ_{Text}) were calculated to be $\gamma_{Glass}\approx71.8$, $\gamma_{BarePEG}\approx63.6$, and $\gamma_{Text}\approx34.1$ mN/m, respectively. Contact angle values are presented as mean values. Surface energy calculations are based on mean contact angles and were calculated using the GGFY model

glass was found to be 9.3° (SD≈3.2°; n=12), but approached 0° when the substrate was hydroxylated by cleaning in a mixture of sulfuric acid and hydrogen peroxide or an oxygen plasma. The contact angle of water on unpatterned PEGDMA was found to be 29.6° (SD≈5.7°; n=8), which was slightly higher than that reported by Kim et al. (Kim et al. 2005), who reported a contact angle of water on PEGDMA to be approximately 22.5° (no SD reported); this discrepancy in the contact angle for unpatterned PEGDMA could be due to any number of reasons (e.g. slightly different polymer chemistry, cleanliness of surface, surface hydration, volume of sessile drop, spreading due to drop distance, etc.). The contact angle of water on the micro-well PEGDMA surface was higher at 68.4° (SD≈8.4°), which demonstrates that the presence of the micro-wells makes the surface quite a bit more hydrophobic.

As discussed in Kim et al. (2005), the increased hydrophobicity of a patterned surface is most likely due to the air pockets that exist in or between structures on a patterned surface (the Cassie state Cassie and Baxter 1944); here, the micro-wells serve as small air pockets between PEGDMA surface area. Cassie et al. (1944) reported that the contact angle of a porous (micro-patterned) surface is theoretically related to the contact angle of a non-porous surface of the same material by Eq. (1) (also demonstrated by Kim et al. 2005).

$$\cos\theta_{\text{Text}} = f_1 \cos\theta - f_2 \tag{1}$$

In Eq. (1), θ_{Text} is the contact angle on a micro-textured surface, θ is the contact angle on a bare unpatterned surface, f_1 is the fractional area of solid surface, and f_2 is the fractional area of air due to the presence of air pockets. It should be noted that $f_1 + f_2$=1 (Kim et al. 2005). For the micro-well array, f_1 is the fraction of unpatterned PEGDMA and f_2 is the fraction of area consumed by the micro-wells, which represent air pockets or porosity in the surface. If we set f_1=0.68 and f_2=0.32 to represent our micro-textured surface and utilize the above reported contact angle θ≈29.6° for bare PEGDMA, we obtain θ_{Text}≈74°, which agrees closely with our measured averaged contact angle of 68.4° and is within one standard deviation (SD=8.4°, n=30).

3.3 Surface energy of PEGDMA micro-well surface

Contact angle is symbolically related to surface energy as (Adamson 1982):

$$\text{surface energy } \gamma_{\text{SV}} = F^{-1}(\text{contact angle } \theta_{\text{S}}, \text{surface tension of test liquid } \gamma_{\text{LV}})$$

where F^{-1} represents an inverted functional relationship. If we have a value for the contact angle of a test fluid on a particular solid surface and the surface tension of that test fluid, we can backsolve to find the surface energy of the surface given an appropriate theoretical model. To estimate surface energies for glass, bare PEGDMA, and our micro-textured PEGDMA surface, we employ the Girifalco–Good–Fowkes–Young (GGFY) model (Girifalco and Good 1957) given by:

$$[1\cos(\theta_{\text{S}})]\cdot\gamma_{\text{LV}} = 2\sqrt{(\gamma_{\text{SL}}\gamma_{\text{LV}})} - \pi \tag{2}$$

π is the vapor pressure, which is assumed to be approximately zero (π≈0) in our calculations, and θ_{S}=contact angle of the surface in question. Since water is used as the test fluid, we can use the known value for the surface tension of water in air at room temperature, γ_{LV}≈72.8 mN/m. From Eq. (2), we estimate the surface energy of the micro-

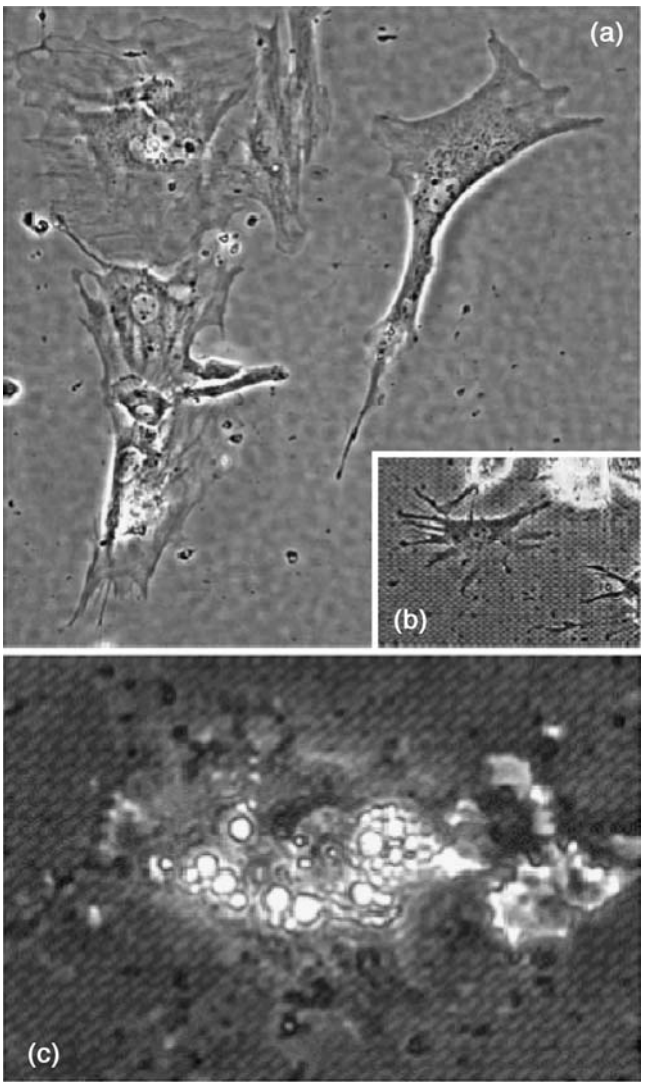

Fig. 4 PAs seeded on (**a**) a glass slide and (**b**) micro-textured PEG (500 nm×4 μm wells, see Fig. 2). Both images are at 200× magnification for direct comparison. (**c**) PA undergoing differentiation as evidenced by lipid loading

textured surface to be $\gamma_{Text} \approx 34.1$ mN/m. In a similar manner, we estimate the surface energy of bare PEGDMA and glass to be $\gamma_{BarePEG} \approx 63.6$ mN/m and $\gamma_{Glass} \approx 71.8$ mN/m, respectively, based on our contact angle data. Our calculation for the surface energy of glass is consistent with published data and lies between those reported for perfectly clean glass (~73 mN/m) and ordinary glass (~70 mN/m; Adamson 1982). Figure 3 summarizes the results of our surface energy calculations. It is important to note that the value for surface energy calculated using the GGFY model is approximate. Employing different models (e.g., Zisman, Owens–Wendt, Wu Harmonic Mean, Lewis Acid–Base Theory) may yield different, yet still approximate, results.

3.4 PAs interacting with micro-wells

Physical topographical cues within the extracellular microenvironment can influence cellular responses including attachment and adhesion, migration, differentiation, as well as the production of new tissue. Due to the lack of available biological or clinical data in the literature supporting the interaction of PAs with sub-micron (<1 μm) texture, an initial study was conducted to investigate this interaction. Rat PAs were harvested and cultured as previously described by us (Patel et al. 2005; Patrick et al. 1999, 2002). The PEGDMA was derivatized with collagen I (Yim et al. 2007). Cells were cultured on both glass (control) and the patterned PEGDMA. Figure 4(a) and (b) illustrate a distinct difference in cell morphology between control and microtextured PEG (magnification is the same).

In the control case, the PAs are quite spread out, displaying conventional morphology observed on glass and tissue culture plastic surfaces. In contrast, PAs on the PEG micro-wells are more confined and appear to have cell processes adherent to the micro-well structures. The cell pattern observed in Fig. 4(b) is very reminiscent of

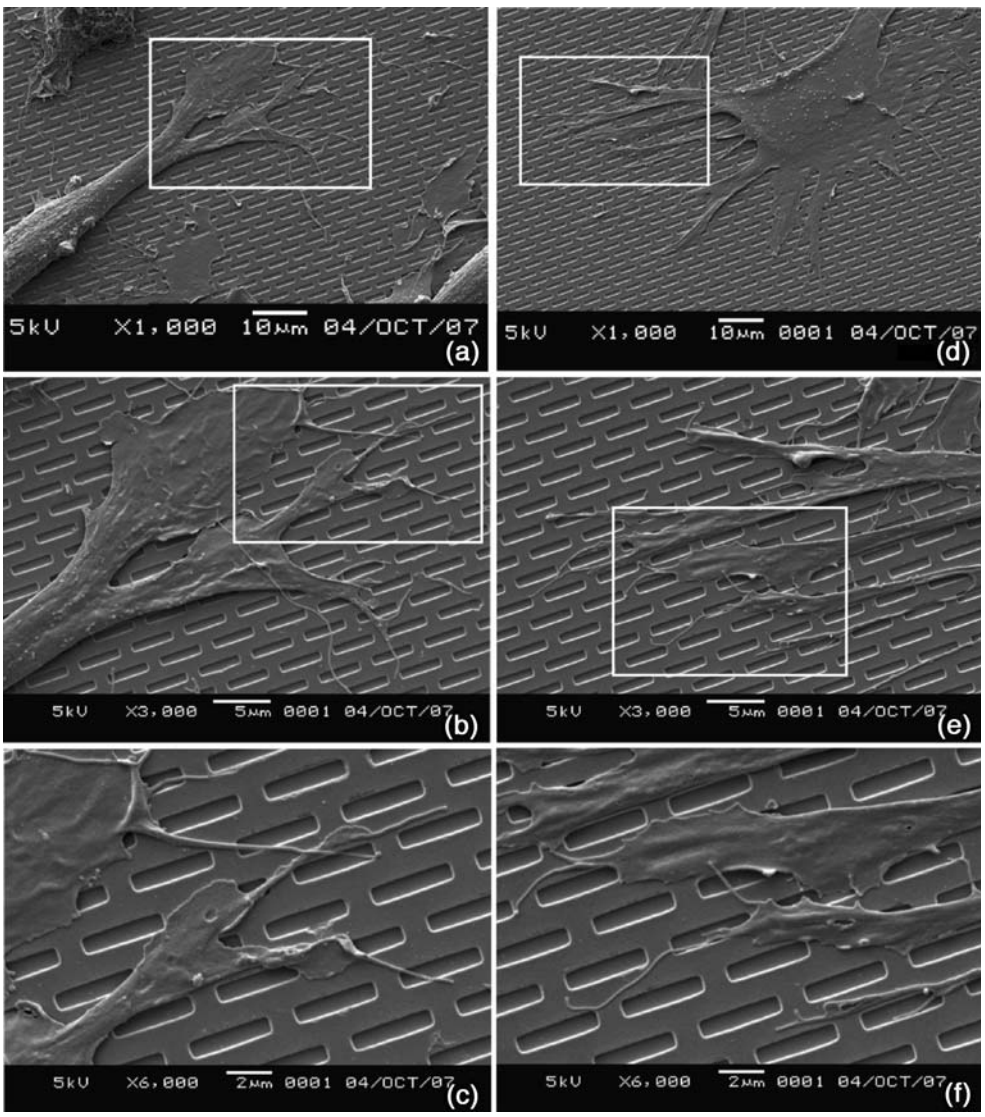

Fig. 5 SEM images of PAs on the biofunctionalized, PEG micro-well array. Individual cell processes and cell membranes interact with the micro-well topography, growing into the micro-wells. (**a**–**c**) and (**d**–**f**) depict the same area at different magnifications. *White boxes* denote magnified area. (**a**, **d**) 1,000×. (**b**, **e**) 3,000×. (**c**, **f**) 6,000×

keratinocytes grown on micro-pillar structures derivatized with fibronectin (Steinberg et al. 2007). The micro-wells seem to provide traction for the PAs to the PEG as the added surface area provides gripping to the cells' processes. The morphological confinement of the cells on the micro-wells relative to those on the control glass is consistent with the surface energy calculations of Fig. 3. As contact angle decreases or surface energy increases, the PAs cell body tend to spread out; to the contrary, the PAs cell body tend to curl up on surfaces with a low surface energy.

In addition to morphological changes, individual PAs were observed to undergo differentiation (Fig. 4(c)), a process that normally occurs only after PAs are surrounded by other PAs. This is evident by lipid-loading or the coalescence of lipid droplets (bright spots) within the PA in Fig. 4(c). The SEM images in Figs. 5 and 6 demonstrate individual cell processes and cell membranes interacting and, in fact, growing into the micro-wells. The white boxes in Figs. 5 and 6 show magnified areas (see figure captions). Because the dimensions of the cell processes of the PAs are smaller than the micro-well structures, decreases in effective surface energy due to the air gaps in the micro-well topography have intrinsically little affect on the processes' conformation; however, changes in surface energy due to the presence of nanoscale topography, where the dimension of the processes is larger than the air gaps in the surface, would seemingly affect the conformation of the cell processes since the nanofeatures are too small for the processes to grow into. For the micro-well surface, the conformation of the cell processes is affected by the added surface area due to the presence of the micro-wells, which effectively increases the density of surface area in the horizontal plane of the PEGDMA surface.

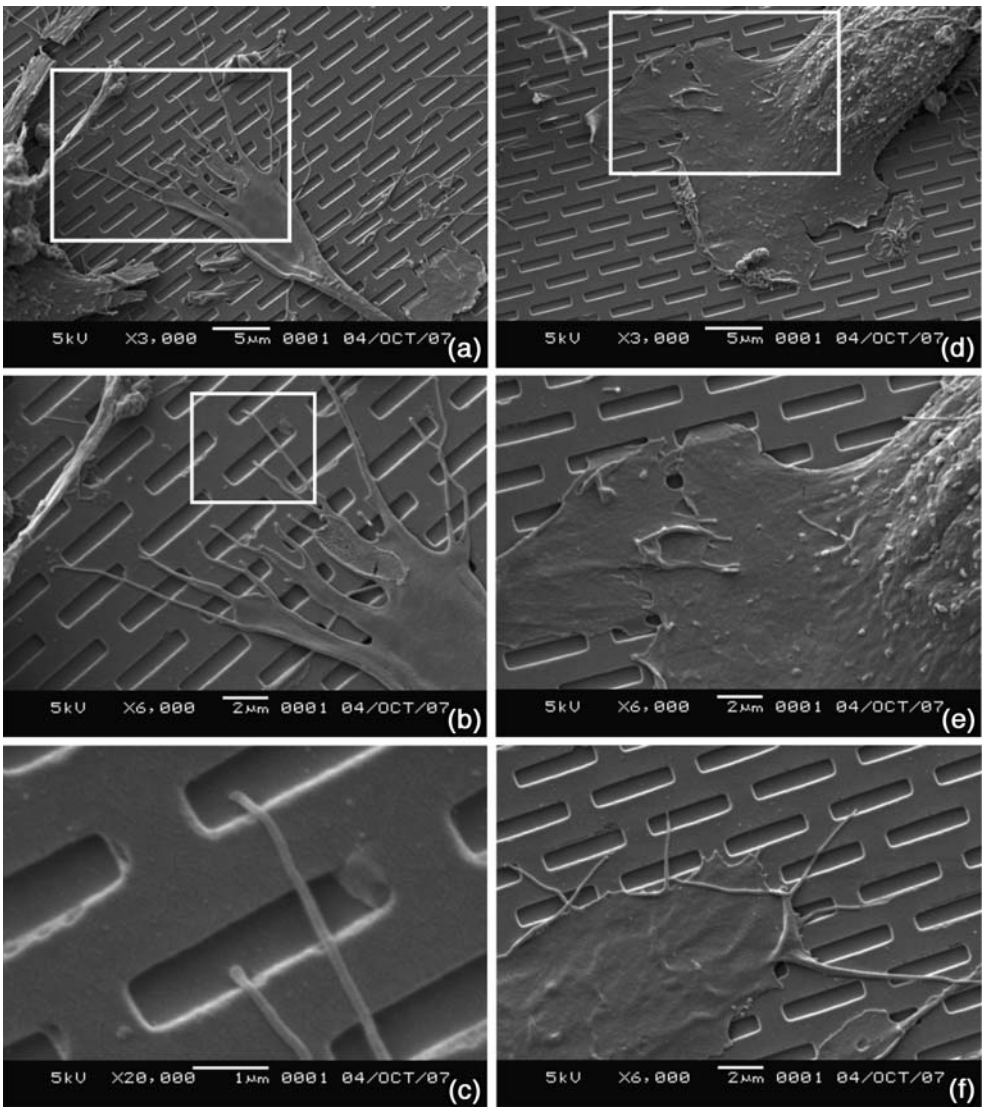

Fig. 6 SEM images of PAs on a biofunctionalized, PEG micro-well array. Individual cell processes and cell membranes interact with the micro-well topography, growing into the micro-wells. (**a**–**c**) and (**d**–**e**) depict the same area at different magnifications. *White boxes* denote magnified area. (**a**, **d**) 3,000×. (**b**, **e**, **f**) 6,000×. (**c**) 20,000×

4 Conclusions

Here, we study the qualitative affects of a tread-like micro-well topography in PEGDMA on the morphology and behavior of PAs in culture. The micro-well texture is patterned in the PEGDMA using the FILM nanomanufacturing process. We are the first to employ FILM for a tissue engineering application and found that it was more convenient than other imprinting processes like S-FIL and UV-NIL and 365 nm *i*-line photolithography. The FILM process was able to imprint the micro-well texture with high fidelity over a large area while only requiring the use of common mask aligner technology available in most cleanrooms and a cheap silicon imprinting mold. Contact angle and surface energy analysis were performed to characterize the micro-well scheme; the analyses demonstrated that the presence of the micro-wells in the PEGDMA increases hydrophobicity. According to theory, the increase in hydrophobicity of the micro-well surface is due to the micro-wells mimicking small air pockets in the solid PEGDMA surface.

Our studies demonstrate that PAs uniquely interact with the micro-well PEGDMA surfaces derivatized with Collagen I, and that cell behavior is qualitatively modulated compared with planar control surfaces. Observation from cell culture is consistent with changes in hydrophobicity demonstrated by the surface energy calculations. We believe that the micro-well topography may be useful in implantable adipose tissue scaffolds in modulating PA-response and tissue formation. Our further work will be devoted to performing competition assays to determine the types of physical micro- and nanotopographies that PAs most prefer in an effort to more thoroughly understand the design aspects of implantable adipose tissue scaffold fabrication. We will also be investigating the effects of varying mechanical properties of PEGDMA and the addition of adhesion peptides and other biochemistry (e.g., growth factor) on PA behavior.

Acknowledgements We acknowledge the technical assistance of Ms. Krithi Mittakanti during her summer internship. This work is supported in part by a grant from the Office of Naval Research to SCC. CWP acknowledges the grant from the Susan G. Komen Foundation and a NCI grant CA16672 awarded to M. D. Anderson Cancer Center. Work was performed in part at the Center for Nano and Molecular Science and Technology (CNM) and at the Microelectronics Research Center (MRC), a part of the National Microfabrication Infrastructure Network supported by NSF at UT-Austin.

References

G.A. Abrams, S.L. Goodman, P.F. Nealey, M. Franco, C.J. Murphy, Nanoscale topography of the basement membrane underlying the corneal epithelium of the rhesus macaque Cell Tissue Res. **299**, 39 (2000) DOI 10.1007/s004410050004

A.W. Adamson (ed.), (s), Physical chemistry of surfaces, New York, John Wiley and Sons, 1982

A.W. Adamson, F.P. Shirley, K.T. Kunichika, Contact angles on molecular solids: I. Ice J. Colloid Interface Sci. **34**, 461 (1970) DOI 10.1016/0021-9797(70)90206-7

J.M. Andreas, E.A. Hauser, W.B. Tucker, Boundary tension by pendant drops J. Phys. Chem. **42**, 1001 (1938) DOI 10.1021/j100903a002

S. Asai, Y. Kamei, K. Nishibori, T. Katoh, S. Torii, Reconstruction of Romberg disease defects by omental flap Ann. Plast. Surg. **57**, 154 (2006 DOI 10.1097/01.sap.0000216243.91162.c2

E. Billings Jr., J.W. May Jr., Historical review and present status of free graft autotransplantation in plastic and reconstructive surgery Plast. Reconstr. Surg. **83**, 368 (1989) DOI 10.1097/00006534-198902000-00033

A.B.D. Cassie, S. Baxter, Wettability of porous surfaces Trans. Faraday Soc. **40**, 546 (1944) DOI 10.1039/tf9444000546

M. Colburn, S. Johnson, M. Stewart, S. Damle, T. Bailey, B.J. Choi, et al, *Step and Flash Imprint Lithography: A New Approach to High-Resolution Patterning*, Proceedings of the SPIE's 24th International Symposium on Microlithography: Emerging Lithographic Technologies III, Santa Clara, CA, March 1999, **3676**, 379.

R.A. Ersek, Transplantation of purified autologous fat: A 3-year follow-up disappointing Plast. Reconstr. Surg. **87**, 219 (1991)

F.M. Fowkes, W.D. Harkins, The state of monolayers adsorbed at the interface solid–aqueous solution J. Am. Chem. Soc. **62**, 3377 (1940) DOI 10.1021/ja01869a029

D.Y. Fozdar, W. Zhang, M. Palard, C.W. Patrick Jr., S.C. Chen, Flash imprint lithography using a mask aligner (FILM): a method for printing nanostructures in photosensitive hydrogels for tissue engineering Nanotechnology **19**, 215313 (2008) DOI 10.1088/0957-4484/19/21/215303

L.A. Girifalco, R.J. Good, A theory for the estimation of surface and interfacial energies. I. derivation and application to interfacial tension J. Phys. Chem. **61**, 904 (1957) DOI 10.1021/j150553a013

J.A. Hunt, P.C. Hobar, Common craniofacial anomalies: conditions of craniofacial atrophy/hypoplasia and neoplasia Plast. Reconstr. Surg. **111**, 1497 (2003) DOI 10.1097/01.PRS.0000049646.25757.BE

P. Kim, D.H. Kim, B. Kim, S.K. Choi, S.H. Lee, A. Khademhosseini et al., Fabrication of nanostructures of polyethylene glycol for applications to protein adsorption and cell adhesion Nanotechnology **16**, 2420 (2005) DOI 10.1088/0957-4484/16/10/072

P.N. Patel, A.S. Gobin, J.L. West, C.W. Patrick, Poly(ethylene glycol) hydrogel system supports preadipocyte viability, adhesion, and proliferation Tissue Eng. **11**, 1498 (2005) DOI 10.1089/ten.2005.11.1498

C.W. Patrick, Adipose tissue engineering: the future of breast and soft tissue reconstruction following tumor resection Semin. Surg. Oncol. **19**, 302 (2000) DOI 10.1002/1098-2388(200010/11)19:3<302::AID-SSU12>3.0.CO;2-S

C.W. Patrick, Tissue engineering strategies for adipose tissue repair Anat. Rec. **263**, 361 (2001) DOI 10.1002/ar.1113

C.W. Patrick, P.B. Chauvin, J. Hobley, G.P. Reece, Preadipocyte seeded PLGA scaffolds for adipose tissue engineering Tissue Eng. **5**, 139 (1999) DOI 10.1089/ten.1999.5.139

C.W. Patrick, B. Zheng, C. Johnston, G.P. Reece, Long-term implantation of preadipocyte-seeded PLGA scaffolds Tissue Eng. **8**, 283 (2002) DOI 10.1089/107632702753725049

N. Sniadecki, R.A. Desai, S.A. Ruiz, C.S. Chen, Nanotechnology for cell-substrate interactions Ann. Biomed. Eng. **34**, 59 (2006) DOI 10.1007/s10439-005-9006-3

T. Steinberg, S. Schulz, J.P. Spatz, N. Grabe, E. Mussig, A. Kohl et al., Early keratinocyte differentiation on micropillar interfaces Nano Lett. **7**, 287 (2007) DOI 10.1021/nl062271z

L. Vaienti, M. Soresina, A. Menozzi, Parascapular free flap and fat grafts: combined surgical methods in morphological

restoration of hemifacial progressive atrophy Plast. Reconstr. Surg. **116**, 699 (2005) DOI 10.1097/01.prs.0000177449.12366.48

X.C. Wang, Q. Qiao, Z.F. Liu, R. Zhao, H.L. Zhang, Y.J. Yang et al., Free anterolateral thigh adipofascial flap for hemifacial atrophy Ann. Plast. Surg. **55**, 617 (2005) DOI 10.1097/01.sap.0000189659.76694.e2

E.K.F. Yim, R.M. Reano, S.W. Pang, A.F. Yee, C.S. Chen, K.W. Leong, Nanopattern-induced changes in morphology and motility of smooth muscle cells Biomaterials **26**, 5405 (2005) DOI 10.1016/j.biomaterials.2005.01.058

E.K.F. Yim, S.W. Pang, K.W. Leong, Synthetic nanostructures inducing differentiation of human mesenchymal stem cells into neuronal lineage Exp. Cell Res. **313**, 1820 (2007)